Multiple-Doppler Radar Network Design

PETER S. RAY AND KAREN L. SANGREN[1]

National Severe Storms Laboratory, Norman, OK 73069

(Manuscript received 11 January 1983, in final form 21 April 1983)

ABSTRACT

Observing programs utilizing Doppler radars must have them deployed in optimum locations to best satisfy experimental objectives and maximize economies. One wishes to determine the coordinate triples (x_i, y_i, z_i), where i equals the number of radars, which maximize the value of the data to be collected. The optimum location is governed by a value or objective function. Here, possible networks of two to nine radars are given for two different error specifications. The objective functions with both error distributions maximize the quantity (AREAL COVERAGE/ERROR). The procedure is to search the finite number of local maxima for the global maximum in the value of the objective function. This is done by employing a searching algorithm at each of a number of starting vectors which are close enough to the local maxima to converge to the desired local maxima. In all cases, the network obtained by considering all radars simultaneously is superior to that obtained by combining optimum smaller sub-networks. Our results suggest the expected benefits for networks with additional constraints, reflecting the more complex experimental objectives particular to some individual field program. For example, the number of radars needed and their optimal configuration can be determined for a field program requiring a specified areal coverage (probability that a desired event will occur) and resolution (to retrieve a specified scale of motion).

1. Introduction

Resource limitations and individual scientific objectives in multipurpose large field programs require efficient and planned use of facilities. Most, if not all, experimental objectives would be satisfied by instantaneous high resolution measurements over a large region of space with high accuracy. However, the need to cover a reasonably large volume requires radar locations which are far apart, whereas accuracy and resolution are maximized by radar locations close together. This study examines the corresponding network design problem.

Relationships among areal coverage, spatial resolution, and accuracy of horizontal velocity measurements for two radars (dual-Doppler radar) were examined by Davies-Jones (1979). From the relations Davies-Jones presented, one can form a value function which would dictate the radar spacing and with additional information, the orientation. It is possible to determine optimum radar placement (separation) if one of the three variates can be disregarded from the presented nomograms. The advantages of a three- (or more) radar network over a two-radar network are given in Ray and Wagner (1976). In summary, as the number of radars is increased, the limitations of a two-radar network are mitigated by extending areal coverage while simultaneously increasing the integrated reliability. This work was extended in Ray *et al.* (1978) to include up to five Doppler radars. It was demonstrated that the optimum network is not produced by adding an additional radar (even in an optimal way) to an existing optimum network.

Up to seven Doppler radars were included in a study by Ray *et al.* (1979) that formed the basis for radar locations for the SESAME program. Again, the basis for radar location was the use of a value or objective function. This function maximized the quotient (AREAL COVERAGE/ERROR).

The present study extends these results by (1) examining two formulations of the objective function and (2) by including a constraint requiring specified resolution.

2. Optimal siting algorithm

If x_i, y_i, z_i represent the coordinates of the ith radar with respect to an arbitrary origin, and the radar is viewing particle motion with components u, v, and $W(=w+V_t)$ in the x, y, and z directions, respectively, then the measured radial velocity V_i at the coordinate triple (x, y, z) is given by

$$u(x - x_i) + v(y - y_i) + W(z - z_i) = V_i R_i, \quad (1)$$

when

$$R_i = [(x - x_i)^2 + (y - y_i)^2 + (z - z_i)^2]^{1/2}, \quad (2)$$

where V_t is the particle terminal velocity determined from radar reflectivity and w is the vertical component of air motion.

Radial velocity estimates from three non-colinearly located radars are sufficient to determine the particle

[1] Cooperative Institute for Mesoscale Meteorological Studies (CIMMS), University of Oklahoma, Norman.

motion components in Eq. (1). Additional radars result in an overdetermined system. If the discrepancy sum of squares

$$I = \sum_i [\hat{u}(x - x_i) + \hat{v}(y - y_i) + \hat{W}(z - z_i) - V_i R_i], \quad (3)$$

is minimized for all i, a least-squares estimate of the particle motion $(\hat{u}, \hat{v}, \hat{W})$ is found which represents the maximum likelihood estimate if the errors are normally distributed. The inclusion of additional radars results in a more accurately determined wind field. Normal equations can be derived from Eq. (3) in the matrix form [**C**][**X**] = [**A**] by setting $\partial I/\partial \hat{u} = \partial I/\partial \hat{v} = \partial I/\partial \hat{w} = 0$. In this form

$$\begin{pmatrix} \sum (x-x_i)^2 & \sum (x-x_i)(y-y_i) & \sum (x-x_i)(z-z_i) \\ \sum (x-x_i)(y-y_i) & \sum (y-y_i)^2 & \sum (y-y_i)(z-z_i) \\ \sum (x-x_i)(z-z_i) & \sum (y-y_i)(z-z_i) & \sum (z-z_i)^2 \end{pmatrix} \begin{pmatrix} u \\ v \\ W \end{pmatrix} = \begin{pmatrix} \sum V_i(x-x_i)R_i \\ \sum V_i(y-y_i)R_i \\ \sum V_i(z-z_i)R_i \end{pmatrix}, \quad (4)$$

where the coefficient matrix [**C**] is symmetric and whose inverse is denoted by [**B**] = [**C**]$^{-1}$. If σ_{vi}^2 is the error variance in the radial velocity estimate from the ith radar, then the variances of the estimator of the synthesized wind components are given by

$$\begin{pmatrix} \sigma_u^2 \\ \sigma_v^2 \\ \sigma_w^2 \end{pmatrix} = \begin{pmatrix} \sum \sigma_{vi}^2(B_{11}(x-x_i)R_i + B_{12}(y-y_1)R_i + B_{13}(z-z_i)R_i)^2 \\ \sum \sigma_{vi}^2(B_{12}(x-x_i)R_i + B_{22}(y-y_i)R_i + B_{23}(z-z_i)R_i)^2 \\ \sum \sigma_{vi}^2(B_{13}(x-x_i)R_i + B_{23}(y-y_i)R_i + B_{33}(z-z_i)R_i)^2 \end{pmatrix}. \quad (5)$$

A second method of obtaining wind estimates is given in Ray *et al.* (1980b). Wind estimates are determined directly on a Cartesian grid from two Doppler radars by invoking the equation of continuity

$$\frac{\partial u}{\partial x} + \frac{\partial v}{\partial y} + \frac{\partial w}{\partial z} - \kappa w = 0, \quad (6)$$

where κ is the logarithmic rate of change of density with height. This was generalized by Kessinger (1983) for arbitrary (≥ 2) number of radars. The functional I in Eq. (3) is treated in standard least squares methodology to obtain the u and v components. Each of these are expressed in terms of the other two orthogonal wind components. By substituting the v-solution into the u-equation and the u-solution into the v-equation we obtain separate equations for the u and v component in terms of the measured radial velocities, position of the radar with respect to the observations, and the vertical wind (and particle fall speed) components. The initial w guess is taken from an adjacent (in the vertical) vertical velocity value. As shown by Kessinger, this formulation generally provides more accurate wind estimates over a larger area than the solution of Eq. (4) if boundary conditions are reasonably well known. The resulting equations for u and v are

$$u = \frac{\sum R_i V_i(x-x_i) \sum (y-y_i)^2 - \sum R_i V_i(y-y_i) \sum (x-x_i)(y-y_i)}{\sum (x-x_i)^2 \sum (y-y_i)^2 - [\sum (x-x_i)(y-y_i)]^2} + \frac{W[\sum (y-y_i)(z-z_i) \sum (x-x_i)(y-y_i) - \sum (y-y_i)^2 \sum (x-x_i)(z-z_i)]}{\sum (x-x_i)^2 \sum (y-y_i)^2 - [\sum (x-x_i)(y-y_i)]^2}, \quad (7a)$$

$$v = \frac{\sum R_i V_i(y-y_i) \sum (x-x_i)^2 - \sum R_i V_i(x-x_i) \sum (x-x_i)(y-y_i)}{\sum (y-y_i)^2 \sum (x-x_i)^2 - [\sum (x-x_i)(y-y_i)]^2} + W\frac{[\sum (x-x_i)(y-y_i) \sum (x-x_i)(z-z_i) - \sum (x-x_i)^2 \sum (y-y_i)(z-z_i)}{\sum (y-y_i)^2 \sum (x-x_i)^2 - [\sum (x-x_i)(y-y_i)]^2}. \quad (7b)$$

The vertical component of air motion w and refined estimates of u and v are determined then from (6) and (7a) and (7b) through iteration.

The variance of the estimator of the deduced wind component can then be expressed as

$$\sigma_u^2 = \{\sum_i \sigma_{v_i}^2[R_i(x-x_i)(\sum (y-y_i)^2) - R_i(y-y_i)(\sum x-x_i)(y-y_i))]^2 + \sigma_W^2[\sum (y-y_i)^2 \sum (x-x_i)(z-z_i) - \sum (x-x_i)(y-y_i) \sum (y-y_i)(z-z_i)]^2\} \times \left\{\frac{1}{\sum (x-x_i)^2 \sum (y-y_i)^2 - [\sum (x-x_i)(y-y_i)]^2}\right\}^2 + \text{cov}(u, w), \quad (8a)$$

$$\sigma_v^2 = \{\sum \sigma_{v_i}^2[R_i(y-y_i)(\sum (x-x_i)^2) - R_i(x-x_i)(\sum (x-x_i)(y-y_i))]^2 + \sigma_W^2[\sum (x-x_i)^2 \sum (y-y_i)(z-z_i) - \sum (x-x_i)(y-y_i) \sum (x-x_i)(z-z_i)]^2\} \times \left\{\frac{1}{\sum (x-x_i)^2 \sum (y-y_i)^2 - [\sum (x-x_i)(y-y_i)]^2}\right\}^2 + \text{cov}(v, w), \quad (8b)$$

where

$$\sigma_W^2 = \sigma_w^2 + \sigma_{v_t}^2$$

and cov(u, w) and cov(v, w) represent terms which involve covariances between u and w, and v and w, respectively. These terms can be shown to be negligible for this analysis. The variance in the vertical velocity estimate is expressed as

$$\sigma_w^2 = \frac{1}{2}\left\{1 + \left(\frac{\frac{1}{\Delta z} - \frac{\kappa}{2}}{\frac{1}{\Delta z} + \frac{\kappa}{2}}\right)^2\right\}\sigma_{w_{k+1/2}}^2 + \frac{\sigma_u^2}{\left[2\Delta x\left(\frac{1}{\Delta z} + \frac{\kappa}{2}\right)\right]^2} + \frac{\sigma_v^2}{\left[2\Delta y\left(\frac{1}{\Delta z} + \frac{\kappa}{2}\right)\right]^2} \quad (8c)$$

for downward integration, where κ is an index denoting height level and derivatives have been approximated by centered differences and the integration approximated through the trapezoidal rule. The $\sigma_{v_t}^2$ is the variance in the fall speed estimate.

An experimental design effort should maximize the use of physical resources as well as the probability that the information sought will be present in the collected data. This requires that the goals and operational constraints be explicitly stated. Factors that may be relevant to the Doppler radar siting problem include: terrain, scan rates, beam broadening, resolution, errors in deduced winds, area of coverage and sidelobes. All of these effects can be quantified and expressed mathematically such that their influence can be included in a value statement that reflects the stated goals of the experiment or field program. The siting problem expressed in this manner then becomes a numerical problem in optimization where the radar locations—the decision variables—are to be chosen such that the value statement, usually termed the objective function, is optimized (maximized or minimized as appropriate). The resulting optimization problem can be solved using the techniques of nonlinear programming drawn from the field of mathematical programming.

Following the discussion in Ray *et al.* (1980a), nonlinear programming applied to the siting problem allows for a solution to a nonlinear objective function while simultaneously forcing the solution to satisfy constraints applicable to the problem, either in the form of equality or inequality relations. Mathematically this is expressed as ${}_x{}^{\text{opt}}[R(x)]$; $x \in E^N$, subject to

$$\left.\begin{aligned} G_j(x) &= 0, \quad j = 1(1)J \\ H_k(x) &< 0, \quad k = 1(1)K \end{aligned}\right\},$$

where x is a column vector in N-dimensional Euclidean space containing the decision variables, R is the objective function, G the J equality constraints, and H the K inequality constraints. The objective function may be either linear or nonlinear. The notation ${}_x{}^{\text{opt}}[R]$ implies optimization of R through the proper choice of x. For the siting problem x contains the radar coordinates and possibly other relevant parameters, for example, scan rate. The constraints can be employed to place bounds on the decision variables, such as guaranteeing that a network is capable of covering a specified area. These can also be used to permit climatological factors to influence the solution. The greatest difficulty with this approach is the formulation of an objective function that reflects the goals of the experiment. This process starts with stating the goals of the program, the requirements needed to achieve these goals and finally, the system characteristics. Since these are usually different for each field program, stating a universal objective function is not possible. However, most researchers would probably agree that the network should have areal coverage as large as possible, with high resolution and small error in the deduced winds. Since most multiple Doppler data are interpolated to an array of grid points, minimization of the interpolation error could also be a factor. Thus, the objective function should contain terms relating the radar coordinates to areal coverage, resolution, and interpolation error.

The objective function (O) is chosen to be the integrated reliability

$$O(x_i, y_i, z_i) = \iint_A \bar{\kappa}\, dx dy, \quad i = 1, \ldots, N\text{—the number of radars}, \quad (9)$$

where

$$\bar{\kappa} = Z_T^{-1} \int_0^{Z_T} \frac{1}{\sigma_{\bar{v}}^2}\, dZ$$

and Z_T is the top of the nominal analysis domain (here 13 km), $\sigma_{\bar{v}}^2 = \sigma_u^2 + \sigma_v^2 + \sigma_w^2$ and the area of integration A is chosen sufficiently large such that the optimization of the objective function is not affected by an increase in area A. Typically the domain in this study was the area encompassed by a square up to 400 km on a side and on the order of ten times larger than the size of the radar array. The important con-

sideration is that it was large enough to contain the data that was considered by all radars in the network. The variances represent the variance in the error estimate of the respective wind components.

Here we consider two specifications of the σ_v^2 error distribution

$$\left.\begin{array}{rl} \text{Case I—Eq. (5):} & 13 \geqslant Z \geqslant 6 \text{ km} \\ \text{Eq. (8):} & 6 \geqslant Z \geqslant 0 \text{ km} \\ \text{Case II—Eq. (8):} & 13 \geqslant Z \geqslant 0 \text{ km} \end{array}\right\} . \quad (10)$$

In the instance that Eq. (8) is used, only two radars are required, additional radars form an overdetermined system with resulting reduction in uncertainty.

In the solution method employed here, an initial placement network is specified (the starting vector) and each radar is moved sequentially to a location which maximizes Eq. (9). After the last radar in the network has been moved, the process is reinitiated. This process is then iterated until any movement of radar position results in a lower value of the objective function. However, although this represents a maximum in the objective function, it may represent only a local maximum. There may be other local maxima which are larger. Thus, all local maxima must be evaluated. (There are a finite number of them; the number depending upon the number of radars.) This process has been automated. Although it could easily be made interactive the computing facilities used for this study are "hostile" to interactive use so it was done through batch processing. All solutions presented here exhibit great symmetry, since we have not included any asymmetric forcing. An example of such forcing might be average storm track, storm climatology, or asymmetric storm structure.

3. Results

Although these results are strictly valid only for the cases presented here, they should have broader applicability since many of the commonly used analysis are quite similar to one of these. Further, since these two cases represent near extremes in methodology, the respective solutions are indicative of the range of feasible radar positions.

a. Case I

For growing convection in which an *a priori* estimate upper boundary condition is possible only with large uncertainty, it may be desirable to use the direct solution (Eq. 5) in the upper portions of the radar analysis. If the direct solution (Eq. 5) were used throughout the depth, the solution would strongly reflect the effects of the vertical velocity uncertainty near the surface as in Ray *et al.* (1979). In fact, the uncertainty in the vertical wind becomes unbounded as the plane defined by the radar locations is approached. Thus, we use the direct solution from storm top to 6 km height and an overdetermined two-Doppler analysis below that height, where the error in the vertical velocity component from the direct solution is excessive.

For all radar positions, the errors from 13 km to 6 km height were computed assuming an interpolated radial velocity error variance as expressed by:

$$\sigma_{v_i}^2 = 0.5\left(\frac{R \text{ (km)}}{30 \text{ (km)}}\right), \quad (11)$$

where R is the distance from the radar to the grid point. A minimum value of 0.1 was required to minimize the effect of the singularity in $\bar{\kappa}$ at $R = 0.0$ km. Terminal velocity error variance $\sigma_{v_t}^2$ was assigned the value of 1.0 m^2 s^{-2}. The error σ_w^2 at 6 km was used for the upper boundary condition in the evaluation of $\bar{\kappa}$ below 6 km using the method outlined in Eq. (8).

The sensitivity of the final radar positions to the formulation of Eq. (11) was tested. First, $\sigma_{v_i}^2$ was assigned a constant value of 0.5 and second, the term in parenthesis in Eq. (11) was squared, reflecting the expected decrease in independent samples with range. In all cases tested, the optimum positions of the radars did not change. Thus, the solution is not expected to vary significantly for error distributions that are within these bounds. Further tests were run to assess the sensitivity to the choice of 6 km as the height of the transition from Eq. (8) to Eq. (5). If the level exceeds 4 km the final location is insensitive to the level. If the transition level exceeds Z_T, then case II is reached. Six km was chosen as representative of this interval and is the level proposed by some researchers who advocate the solution by Eq. (5). The objective function and radar positions are discussed in connection with Fig. 5 and the second objective function.

Fig. 1 shows the areal coverage as a function of the number of radars in the configuration representing the global maximum of the objective function. The spatial dimension of the radar beam may be expressed as $R\theta$ where R is the range, or distance from the radar. The θ represents 3 dB beamwidth, or the angle centered on the beam axis within which power is at least half of peak power. Curves are presented for five spatial beamwidths. In all cases the radars were considered to have angular beamwidths of 0.86°. Only points in which the resolution was at least that specified were used in evaluating the objective function. Resolvable scales in the synthesized wind fields are at least several times larger than $R\theta$ (Srivastava and Atlas, 1974). This is because scales smaller than $R\theta$ are effectively filtered by the beam and several samples are required to define any frequency of an observed phenomenon. The final radar configuration is indicated schematically with each point. The radar separation was empirically determined to be approximately

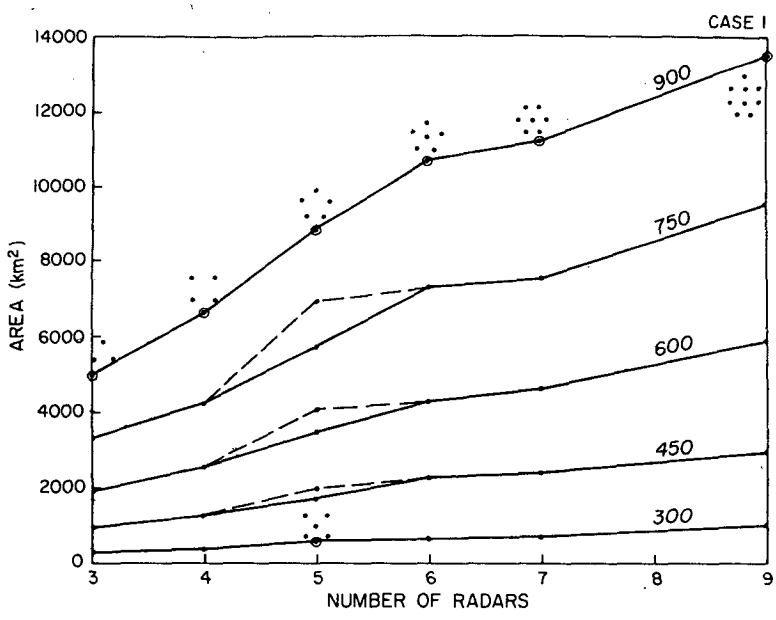

FIG. 1. Optimum radar network (Case 1) coverage area. Each curve includes only the area with spatial resolution less than or equal to the beamwidth (m) as indicated. Dashed curve is for local maximum of objective function which yields the largest area for five radars but with somewhat smaller objective function value.

Radar separation

$$= 40 \text{ (maximum beam dimension)}, \quad (12)$$

where the separation and beam dimension are expressed in km and the radar separation is from one radar to its closest neighbor. Typically, there is about a 10% additional increase in separation as the network increases from 3 to 9 radars. The schematically illustrated positions indicate global maxima in the objective function. In general, there are a finite number of local maxima. These local solutions represent network configurations which cover larger areas but with larger errors or a configuration covering a smaller area with reduced errors when compared to the network with the global maximum in the objective function. In all cases these local maxima are characterized by a smaller value of the objective function. One such case is illustrated below.

There is an increase in area coverage in all cases as the number of radars increases, particularly 4–6 radars and a correspondingly small increase as the number of radars is increased from 6 to 7 radars. From Fig. 1, it is clear that decreasing the required minimum resolution (by, for example, increasing the maximum allowable range) adds as much area as increasing the number of radars. This, of course, is not without penalty. The decrease of resolution is an intolerable cost in many meteorological problems involving Doppler radar networks.

The dashed lines represent locally optimum locations (configurations where the objective function was a maximum or a peak in objective function space for $\partial O/\partial x_i = 0$ where x_i is a space variable in tensor notation), where the network configuration is one with four radars at the verticies of a square with one in the center. The configuration with the highest peak or value of the objective function is represented by the solid line and consisted of radars located at the verticies of a pentagon. Even though the configuration represented by the dashed lines represents a network which covers a larger area, it is shown in Fig. 2 that they are sub-optimal as defined by the chosen objective function.

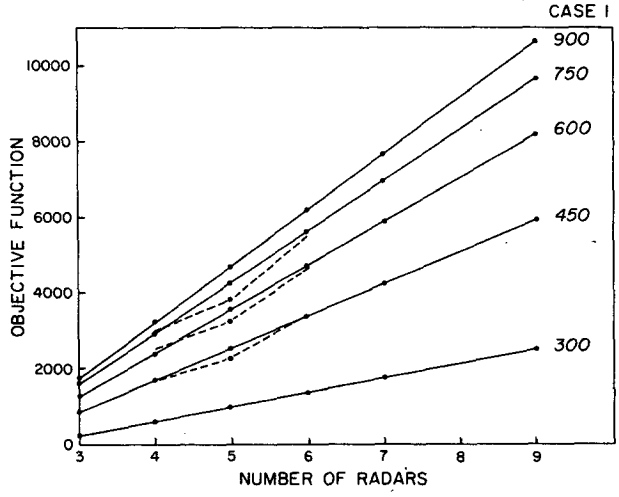

FIG. 2. Maximum objective function value as the number of radars increase for areas encompassed by five beamwidths (m). Dashed line for five radars is objective function value for local maximum which gave the largest area coverage.

The curve for the 300 m beam dimension case does not have a dashed line associated with it because the configuration of 4 radars at the verticies of a square with one in the middle is the objective function's global maximum. In the case of the 900 m beam dimension, no local maximum could be found in the square configuration.

The value of the objective function as a function of the number of radars is shown in Fig. 2 for different beam dimensions. The objective function value (for the optimum network) increases nearly linearly as the number of radars is increased. This means that the added benefit from each additional radar remains constant. Enforcing a constant error, the areal coverage could be made to increase linearly with the number of radars. However, the objective function indicates it is preferable to site all radars simultaneously rather than simply adding optimum sub-networks. Referring to Fig. 1, if the area (for a given resolution) of two three-radar networks is compared to the area of a six-radar network, the difference is, in general, small. The same is true for all other combinations. However, the objective function value for 6 radars is $\sim 3\frac{1}{2}$ times (rather than twice) the value for two three-radar networks. Thus, in addition to doubling the area, the accuracy of the derived fields has been substantially increased within this area. It is this additional benefit that optimization provides.

Dashed lines on the 450, 600, and 750 m beam dimension curves give the objective function value for the five radar configuration of four radars in the corners of a square with one in the middle. The fact that it was a local maximum rather than a global maximum is indicated by its lower objective function value. The increase in area without a corresponding increase in the objective function value means that this configuration is also characterized by generally larger errors in the expected synthesized winds. Other possible networks of five radars, including a combination of three triangles with three radars on one row with two above midway between the three are correspondingly inferior as judged by this objective function.

The areal coverage as a function of beamwidth for the different number of radars is shown in Fig. 3. This shows that the areal coverage increases rapidly as the resolvable wavelength is increased. For a 50% degradation in resolvable scale, one could cover nearly the same area with one-third the number of radars. Inspection of Fig. 3, however, indicates that the resulting fields will not be as accurately determined.

Several network configurations are shown with some of their spatially varying fields for illustration. Figure 4a contains isopleths of the largest beam dimension from the three radars closest to a point. The radar positions were determined by only considering for evaluation all points within the 600 m isopleth. Resolution is illustrated for a larger area to indicate an area at which larger scales might be resolved. For

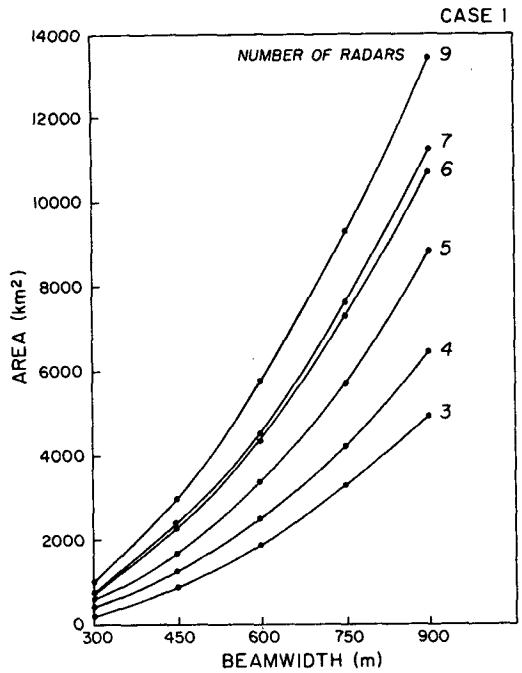

FIG. 3. Increase in areal coverage encompassed by increasing beamwidths. Different curves are for optimum network of three to nine radars.

this network, however, the errors in this extended region would rise sharply over those encompassed by the dashed 600 m isopleth since the network was not designed to accept data beyond that range from any three radars. Expected errors are illustrated in Fig. 4b. Without the area of interest, the errors are generally within 1 $m^2 s^{-2}$.

These figures are contrasted to the less desirable (by our criteria) configuration for five radars. Despite the different geometry, the area encompassed by the dashed line in Fig. 4c is clearly larger than that in Fig. 4a. Again the dashed line encompasses the resolution boundary. From Fig. 4d, the errors within the central 900 km^2 are generally less than 1 $m^2 s^{-2}$ in both cases. However, in the area between the radar location and the resolution boundary, the errors in Fig. 4d increase much more rapidly than in Fig. 4b, thus contributing proportionally less to the objective function, resulting in a lower value objective function since the relative error distribution at all levels is similar to that presented here.

As the number of radars increase, the optimum solution becomes less intuitive. This is illustrated for the case of nine radars in Fig. 4e. The optimum solution was that of a seven-sided polygon with two interior radars. Here the smallest dimension of the beamwidth viewed by at least three radars is a little over 200 m and the area encompassed by 450 m beamwidth is over 3000 km^2. A large fraction of that area is with vertical velocity error at 6 km height of less than 1 $m^2 s^{-1}$ as seen in Fig. 4f.

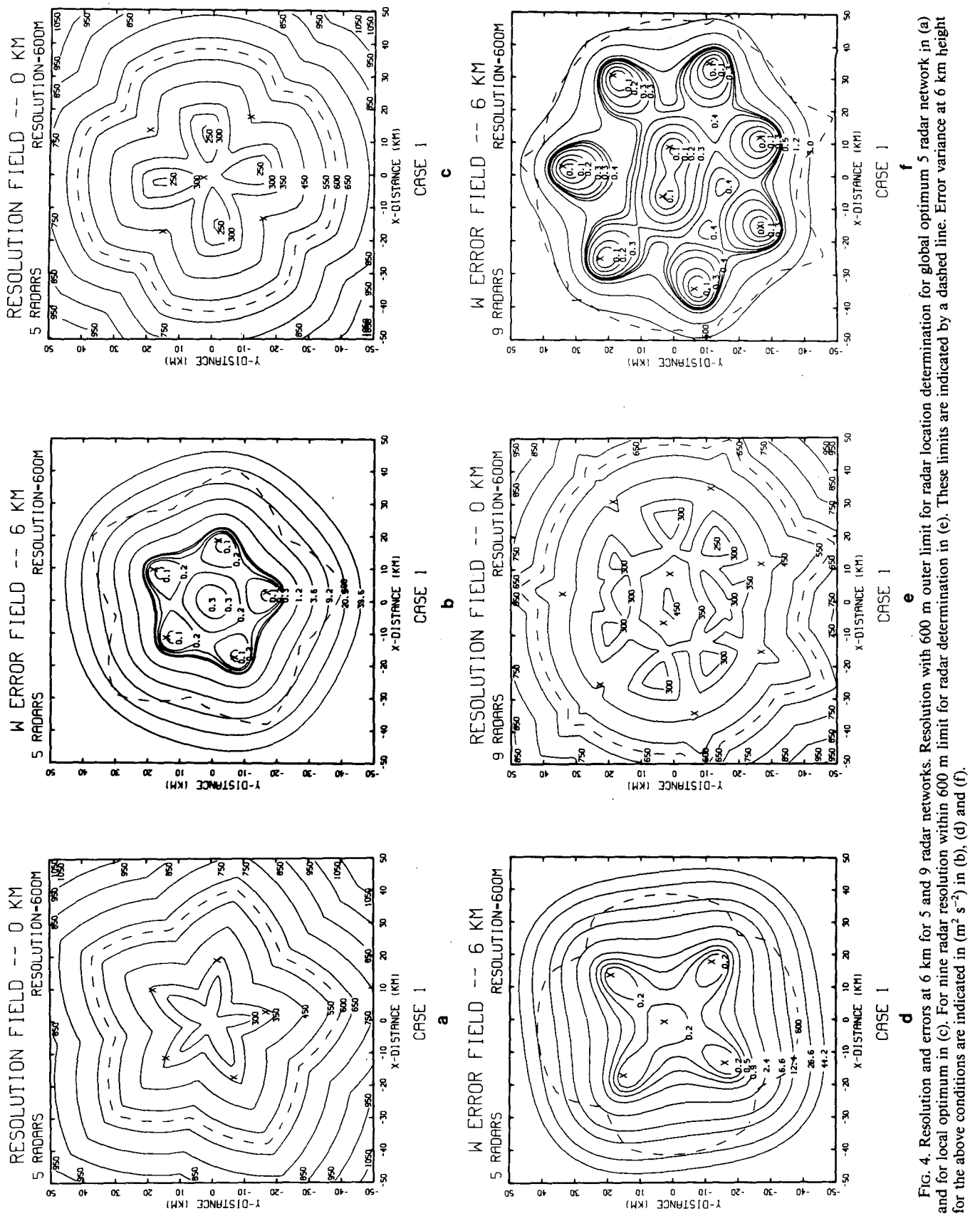

FIG. 4. Resolution and errors at 6 km for 5 and 9 radar networks. Resolution with 600 m outer limit for radar location determination for global optimum 5 radar network in (a) and for local optimum in (c). For nine radar resolution within 600 m limit for radar determination in (e). These limits are indicated by a dashed line. Error variance at 6 km height for the above conditions are indicated in (m^2 s^{-2}) in (b), (d) and (f).

b. Case II

For this case the error formulation of Eq. (8) was used with the objective function represented in Eq. (9). This case requires that a point be within the specified resolution of only two radars, but we must specify a boundary condition error since direct unambiguous measurements of all wind components are not made at any level, except perhaps at the surface. Since Ray *et al.* (1980b) showed the increase in accuracy obtained by downward integration over upward integration, only downward integration is considered.

The process of optimizing the locating radars is illustrated for the case of two radars and a maximum allowable beam dimension of 600 m. If the first radar is fixed at point (0, 0) and the second radar's position is allowed to vary over a square, 80 km on each side, the objective function takes on values as illustrated by the surface in Fig. 5. In this example, the objective function is at maximum at a distance 20 km radius from the first radar. Thus, since there is no asymmetric forcing, the second radar is equally optimally placed at any point on a circle of 20 km radius from the first order. Any point closer or further away from the first radar is less desirable.

As might be expected, with only the requirement that a point be visible to two radars, areal coverage is greatly increased over Case I. Areal coverage is a function of the number of radars as shown in Fig. 6 for five selected resolutions. Comparing the areal coverage found using the second objective function with Fig. 1, the increase in coverage area with two radars is typically a factor of two or more over an analysis requiring three radars. As more radars are added to the network, the coverage area increases more rapidly as the beamwidth (resolution) increases (decreases). The rate of increase appears to be constant with the number of radars.

The effect of choosing an upper boundary condition error of 16 m^2 s^{-2} was tested. Representative cases were run with no boundary error. The resulting optimum network retains the same geometric relationship, but usually the network was expanded such that the distance from a radar to its closest neighbor was increased about 10%. Interestingly, this did not always result in an increase in areal coverage. In fact, the area covered for some experiments decreased even though the area encompassed by the radar positions increased. The relationship given in Eq. (12) approximates the interradar separation for Case II. In some cases the separation was about 10% larger.

A colinear starting vector was used for three radars. Only for the 450 m resolution could a local maximum

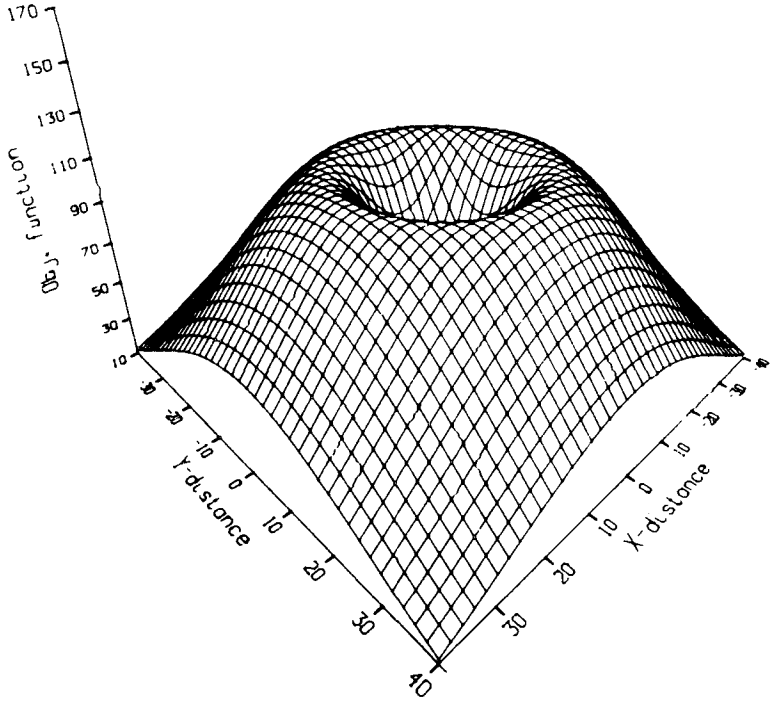

FIG. 5. Three-dimensional plot of objective function value for all considered locations of the second radar. The first radar is located at the origin (0, 0) or the middle of the figure. Optimum location for the second radar is at the objective function maximum (on the rim). The distance between the two, for this case where maximum beam dimension considered is 600 m, is 20 km.

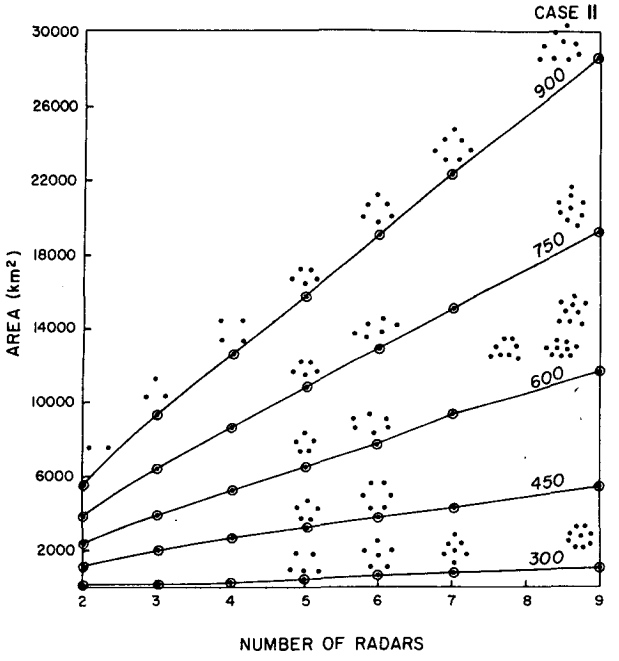

FIG. 6. Optimum radar network (Case II) coverage area. Each curve includes only the area with spatial resolution less than or equal to the beamwidth (m) as indicated.

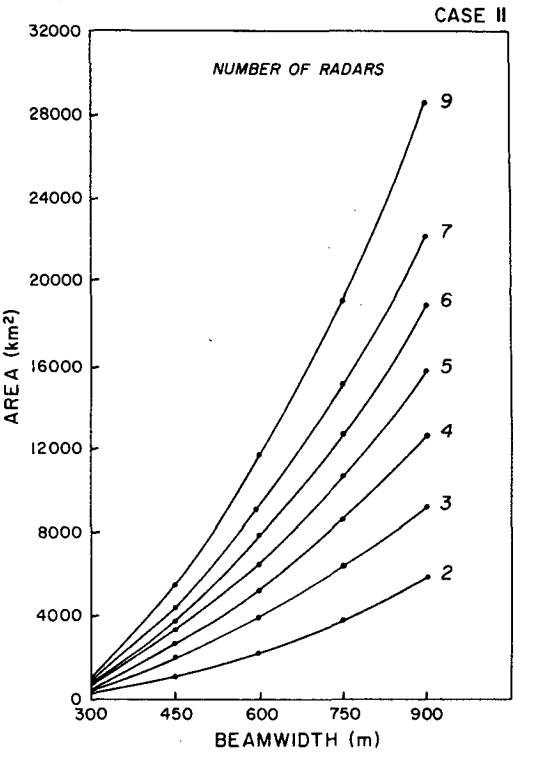

FIG. 8. Increase in areal coverage encompassed by increasing beamwidths. Different curves are for optimum networks of two to nine radars.

be found; for all other experiments, the network moved to an equilateral triangular position which was the global optimum. The clear optimum choice for four radars was a rhombus, very nearly a square. But the five radars solution varied substantially for different starting vectors and resolutions. The optimum networks for Case II generally are symmetric about an axis and each radar is nearly equidistant from as many other radars as possible. In Case I there seemed to be a preference for greater symmetry and less force to locate radar positions equidistant from as many other radars. This preference causes the increase in the optimum objective function as the number of radars is increased in Case II to be less than in Case I.

For nine radars there were several configurations with nearly the same objective function (±5%) and nearly the same area (±5%). In the several local objective function maxima found, the areal coverage was negatively correlated with objective function value.

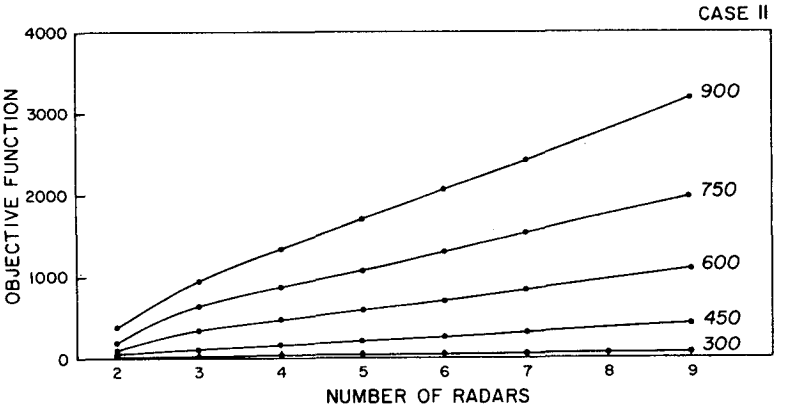

FIG. 7. Maximum objective function value as the number of radars increases for areas encompassed by five beamwidths (m).

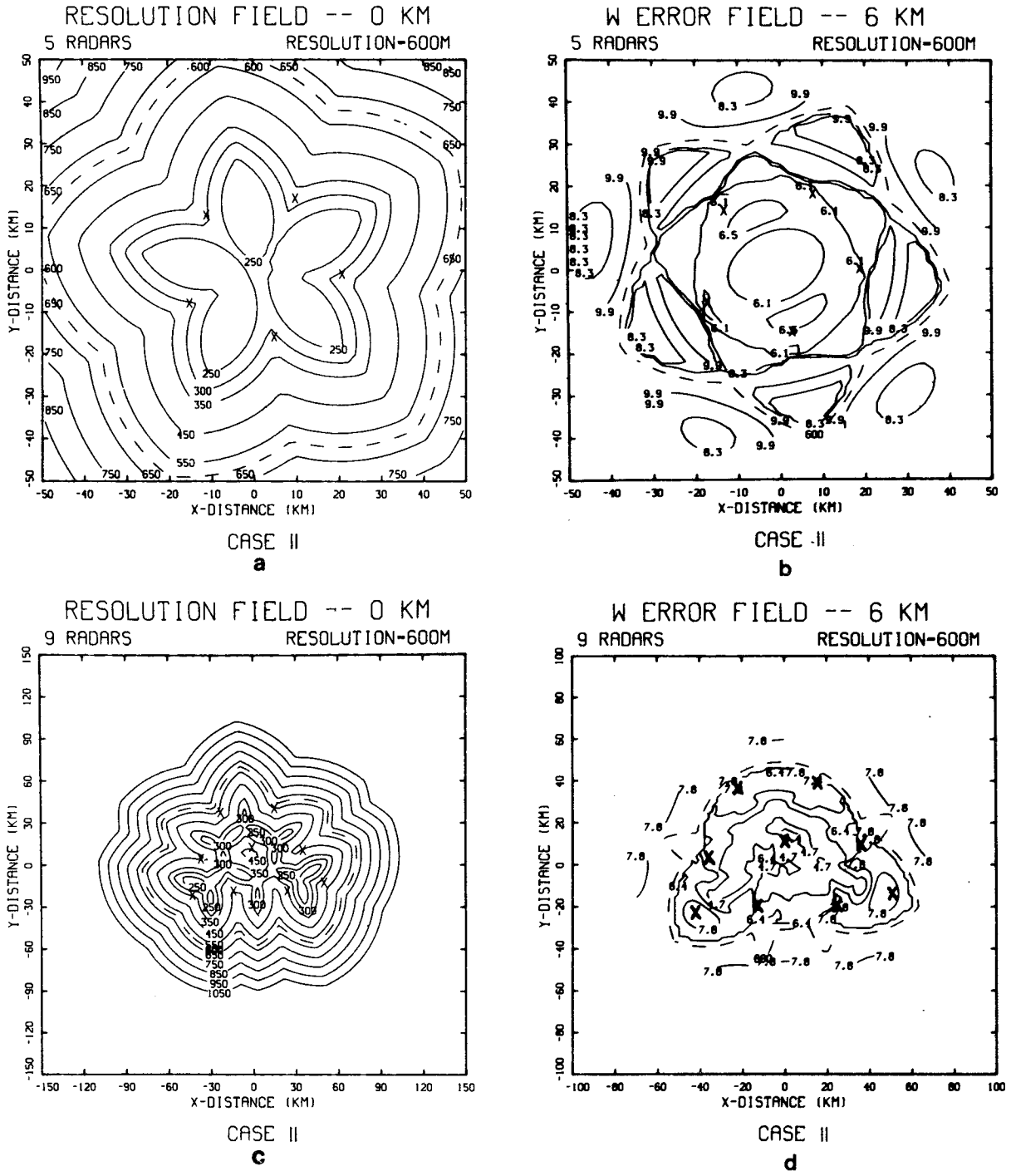

FIG. 9. Resolution and errors at 6 km for five and nine radar networks. Resolution with 600 m outer limit for radar location determination for global optimum is indicated by broken line. Error variance at 6 km height is indicated in (m^2 s^{-2}).

The value of the objective function as the number of radars increases for different beamwidths (resolutions) is shown in Fig. 7 as in Fig. 2. The objective functions increase linearly with the increase in number of radars from 3 to 9 radars. It is not obvious that these or any of the functions plotted should be linear. However, there is a more rapid increase from 2 to 3 radars, implying the gain is greatest with that increase. Since the area increase is linear and the objective function is also linear with additional radars, it follows that the error reduction is constant or linear. Since the objective function increases (slightly) more

rapidly than areal coverage, there must be an error reduction with the increase in radars. This and the fact that areal coverage increases more than it would with just the addition of optimal sub-networks is the result of optimization. The value of the objective function is less than the corresponding network of Case I. This is due to the larger errors associated with Case II. The errors are larger due to the 16 m^2 s^{-2} boundary condition error that was imposed.

The effect of decreasing the resolution requirement on areal coverage for a given number of radars is shown in Fig. 8. Dramatic increases are especially noted as the network consists of a larger number of radars. To optimally sample scales smaller than 1 km the network covers less than 1000 km^2, even with nine radars. However, if experimental objectives can be satisfied with resolvable scales of several kilometers, then it is possible to design a network with a 30-fold increase coverage area. Such trade-offs may be one consideration in formulating an objective function for a proposed experiment. That is, it is possible to design a network such that different resolutions are assumed or to specify a given areal coverage, or both.

The resolution and expected vertical velocity error at 6 km height are shown for five and nine radars in Fig. 9. The shape and area encompassed by the beamwidth for two radars (Case II) is similar to that for three radars (Case I) as shown in Fig. 4a, except the pattern is rotated about the network's center-of-gravity by about 36 (360/10) degrees. As expected, the area encompassing a given resolution is much greater. The isopleths of maximum beamwidth for the two closest radars for a nine radar network is more complex than for five radars. The area encompassed by the radar positions is about 350 m, less than the 450 m evident in Fig. 4e. Although the patterns are different than for Case I, it is generally true that it is possible to resolve a given scale over a larger area in Case II than with the first objective function (Case I).

The anticipated errors in the vertical velocity estimates are in general greater for Case II. This is due to liberal specification of error variance at boundary of 16 m^2 s^{-2}. The spatial distribution of error also is more structured.

4. Summary

Optimization of a radar network will ensure maximizing the probability of meeting experiment objectives and efficiently utilizing observing resources. Each experiment is characterized by unique objectives which will dictate ultimate design details. However, most experiments seek to maximize the coverage area and minimize expected errors with the highest resolution possible. Thus, to develop an understanding for the character of optimum networks with these commonly shared objectives, optimum networks were found for two objective functions. These two evaluation criteria differed in the method of deducing winds, and therefore the associated errors. However, it was found that for networks up to five radars, the siting algorithm was rather insensitive to methods of analysis and error specification. Thus, even though these results are strictly valid only for the two objective functions, it is expected that these results are representative of those for other analysis techniques. An obvious extension of this analysis is to include scanning time and the effects of a given scanning rate. For networks consisting of a large number of radars (>5), several configurations of nearly equal value were found, particularly for the second objective function. Also, it is found that an optimum network has two or three fold advantages over networks which meet minimum requirements, but which are not optimum. It is shown that resolution strongly affects coverage area.

Acknowledgments. The authors acknowledge helpful discussions with Dr. Robert Kropfli and John Cunning. Important contributions were made by Drs. Kenneth Johnson and Dusan Zrnic. The authors acknowledge further constructive comments from Dr. Robert Davies-Jones, Dr. Tzvi Gal-Chen, and reviewer Dr. Robert Serafin. The assistance of Scott Wagner and Matthew Smith in providing results and graphics is also acknowledged. Support for Karen Sangren is through NOAA Grant NA80RAH00004 to the University of Oklahoma.

REFERENCES

Davies-Jones, R. P., 1979: Dual-Doppler radar coverage area as a function of measurement accuracy and spatial resolution. *J. Appl. Meteor.*, **18,** 1229–1233.

Kessinger, C., 1983: An Oklahoma squall line: A multiscale observational and numerical study. Thesis presented as partial fulfillment of Master of Science Degree, University of Oklahoma, 211 pp.

Ray, P. S., and K. K. Wagner, 1976: Multiple Doppler observations of storms. *Geophys. Res. Lett.*, **3,** 189–191.

——, ——, K. W. Johnson, J. J. Stephens, W. C. Bumgarner and E. A. Mueller, 1978: Triple-Doppler observations of a convective storm. *J. Appl. Meteor.*, **17,** 1201–1212.

——, J. J. Stephens and K. W. Johnson, 1979: Multiple-Doppler radar network design. *J. Appl. Meteor.*, **18,** 706–710.

——, M. Gilet and K. W. Johnson, 1980a: The multiple Doppler radar workshop. Part IV: Motion field synthesis and radar placement. *Bull. Amer. Meteor. Soc.*, **61,** 1184–1189.

——, C. L. Ziegler, W. Bumgarner and R. J. Serafin, 1980b: Single- and multiple-Doppler radar observations of tornadic storms. *Mon. Wea. Rev.*, **108,** 1607–1625.

Srivastava, R. C., and D. Atlas, 1974: Effect of finite radar pulse volume on turbulence measurements. *J. Appl. Meteor.*, **13,** 472–480.